JOURNAL OF THERMOPHYSICS AND HEAT TRANSFER
Vol. 18, No. 1, January–March 2004

Thermodynamic Properties of Moist Air: −40 to 400 Degrees Celsius

H. F. Nelson* and H. J. Sauer Jr.†
University of Missouri–Rolla, Rolla, Missouri 65409-0050

The formulations are presented for the thermodynamic properties of moist air at temperatures from −40 to 400°C, humidity ratios from 0 to 1 kg/kg$_{da}$, and pressures ranging from 5529.3 Pa (20-km altitude) to 2 MPa. Moist air is modeled as a real gas using the virial equation of state. Up-to-date values for the virial coefficients of both air and water vapor are used. Equations are derived and results are presented for humidity ratio, specific volume, enthalpy, entropy, wet and dry bulb temperatures, relative humidity, and compressibility. Saturation data are presented for humidity ratio, specific volume, enthalpy, entropy, and compressibility. Results are presented in tabular and graphical form. This work extends the current moist air data to higher temperatures, higher humidity ratios, and a larger range of pressures.

Nomenclature

B_{aa}	=	second virial coefficient, dry air, cm^3/mol
B_{aw}	=	second cross virial coefficient, cm^3/mol
B_m	=	second virial coefficient, mixture, cm^3/mol
B_{ww}	=	second virial coefficient, water, cm^3/mol
C_{aaa}	=	third virial coefficient, dry air, cm^6/mol^2
C_{aaw}	=	third cross virial coefficient, cm^6/mol^2
C_{aww}	=	third cross virial coefficient, cm^6/mol^2
C_m	=	third virial coefficient, mixture, cm^6/mol^2
C_{www}	=	third virial coefficient, water, cm^6/mol^2
f	=	enhancement factor, dimensionless
g, $\bar{g}$	=	Gibbs function, kJ/kg, kJ/kmol
h, $\bar{h}$	=	enthalpy, kJ/kg, kJ/kmol
$h^\circ_{\text{ig},i}$	=	ideal-gas enthalpy, gas i, kJ/kg
M	=	molecular weight, kg/kmol
P, P_s	=	pressure, saturation pressure, Pa
P°	=	1-atm pressure, 101,325 Pa
P_v	=	vapor pressure, Pa
$\bar{R}$	=	universal gas constant, 8.3144 kPa · m^3/kmol · K
s, $\bar{s}$	=	entropy, kJ/kg · K, kJ/kmol · K
$s^\circ_{\text{ig},i}$	=	ideal-gas entropy, gas i at P°, kJ/kg · K
T	=	temperature, K
t	=	dry-bulb temperature, °C
t_{wb}	=	wet-bulb temperature, °C
v	=	specific volume, m^3/kg
W	=	humidity ratio, kg$_w$/kg$_a$
x_a, x_w	=	mole fraction, dry air, water vapor
Z	=	compressibility factor
γ°	=	ideal-gas Gibbs function, nondimensional
ϕ	=	relative humidity, percent

Subscripts

a, or da	=	dry air
as	=	air at saturated water vapor state
dp	=	dew point
i	=	gas i
ig	=	ideal gas
m	=	moist air
s	=	saturation
v	=	vapor
w	=	water vapor
ws	=	saturated vapor

Superscript

-	=	units of per kmol

Introduction

THE humidity content of air must be considered in the design of spacecraft and airplane environmental systems. Turbine engine performance is influenced by the moisture in the incoming air.

When the moisture in humid air condenses, or evaporates, the absorption, or release, of the latent enthalpy of evaporation changes the air temperature. When gas turbines operate in humid conditions the water vapor in the flow can change 1) the ratio of specific heats, 2) the mass flow rate, and 3) the reference speed of sound. Oates[1] gives three high-humidity effects that can occur in a turbine inlet: 1) The mass flow rate in the inlet may be changed because the density of water is so high that any droplets formed due to the lowered static temperature as the air accelerates into the inlet have effectively zero volume; therefore, the condensation allows the inlet mass flow rate to increase. 2) When droplets form, their latent heat of vaporization is released to the surrounding gas, increasing the stagnation temperature of the gas, which tends to reduce the mass flow rate through the inlet. 3) The latent heat of vaporization released by the formation of droplets, reduces the stagnation pressure, which tends to reduce the mass flow rate through the inlet. The net result of these three effects is that, when condensation occurs, the mass flow through the inlet can decrease by 1% or more and the engine thrust is reduced. Thus, substantial variations in engine performance can occur between hot humid days and cool dry days.

Ice formed on aircraft surfaces or on propulsion system surfaces during flight can be extremely hazardous. The possibility of ice or condensation forming on the surfaces of the inlet or the inlet guide vanes of a gas turbine depends on the inlet air temperature and relative humidity. The power produced by turbine engines increases as the temperature of the air entering the compressor decreases. Ice formation in the air or on the inlet surfaces is considered a major concern for the safe operation of any turbine engine because of potential damage to the compressor blades. Stewart[2] developed general inlet air temperature and humidity envelopes for surface icing in turbine inlets.

Presented as Paper 2003-0510 at the 41st Aerospace Sciences Meeting, Reno, NV, 6–9 January 2003; received 17 January 2003; revision received 12 May 2003; accepted for publication 15 May 2003. Copyright © 2003 by the American Institute of Aeronautics and Astronautics, Inc. All rights reserved. Copies of this paper may be made for personal or internal use, on condition that the copier pay the $10.00 per-copy fee to the Copyright Clearance Center, Inc., 222 Rosewood Drive, Danvers, MA 01923; include the code 0887-8722/04 $10.00 in correspondence with the CCC.

*Professor of Aerospace Engineering, Thermal Radiative Transfer Group, Department of Mechanical and Aerospace Engineering and Engineering Mechanics. Associate Fellow AIAA.

†Professor of Mechanical and Aerospace Engineering, Department of Mechanical and Aerospace Engineering and Engineering Mechanics.

Inlet air cooling can be used to increase the performance of both stationary and airplane turbine engines. Evaporative cooling involves the injection of water into the inlet airstream. The water droplets evaporate and cool the inlet air from its dry-bulb temperature to near its wet-bulb temperature. The amount of cooling is limited by the wet-bulb temperature. Andrepont[3] reviewed several concepts for inlet air cooling for combustion turbines and evaluated the concepts as applied to actual electric power plants using stationary combustion turbines.

The hydrogen-fueled air turbo ramjet (ATREX) engine is being considered by the Japanese for a flyback booster for a single-stage-to-orbit space plane.[4] The engine uses a liquid hydrogen heat exchanger to precool the incoming air to increase its thrust and specific impulse to extend its upper Mach number limit. Tanatsugu et al.[4] present icing condition altitude and Mach number envelopes for the ATREX booster based on monthly averages of atmospheric relative humidity.

Balepin and Liston[5] analyzed the concept of turbine engine with inlet air cooling by water injection as a low-cost, low-risk, hypersonic engine capable of achieving Mach 6. Conventional turbojet cycles are restricted to about Mach 3, due to the high air stagnation temperature at the compressor, which begins to reduce compressor performance. Balepin and Liston show that humidity ratios on the order of 0.30 kg_w/kg_a are necessary to keep the compressor inlet temperature less than 400°C at speeds of the order of Mach 6.

The properties of humid air are important in the calibration of microphones and the modeling of friction. Cramer[6] investigated the effect of humidity on the ratio of specific heats and the speed of sound, relative to the calibration of laboratory microphones. He found that an error of 0.001 in the specific heat ratio can cause an error of 0.003 dB in the microphone signal. Crassous et al.[7] investigated and modeled the effect of humidity on the coefficient of friction as a function of velocity and contact time.

Theoretical data are available for the thermodynamic properties of moist air at temperatures up to 200°C and humidity ratios up to 0.09 from the work of Hyland and Wexler[8,9] and Olivieri et al.[10] Very limited theoretical, or experimental data are available at temperatures above 200°C (Ref. 11).

Formulations for the thermodynamic properties of moist air from −60° to 320°C at pressures up to 5 MPa for humidity ratios up to 1 kg_w/kg_a have been developed by Nelson and Sauer[12] and Nelson et al.[13] They treated moist air as a real gas and used the virial equation of state to predict the specific volume, enthalpy, and entropy of both moist air and saturated moist air. The thermodynamic property formulations for moist air were used to generate psychrometric charts at temperatures from 200 to 320°C and pressures from sea level to 5 MPa. Charts were also made for pressures corresponding to altitudes of 750, 1500, and 2250 m at temperatures from 200 to 320°C.

The thermodynamic property formulations for moist air developed by Hyland and Wexler[8,9] were used by Stewart et al.[14] to generate psychrometric charts for sea-level pressure (101.325 kPa) at overlapping temperature ranges of −40–10, 0–50, 10–120, and 100–200°C. Charts were also made for pressures corresponding to altitudes of 750, 1500, and 2250 m at temperatures from 0 to 50°C.

The objective of the research reported herein is to formulate the thermodynamic properties for moist air and to present the properties in the form of tables and psychrometric charts at pressures from 20 atm (2 MPa) to pressures corresponding to 20-km altitude (5529.3 Pa).

Equation of State

Air is assumed to have a composition of 78.12% nitrogen, 20.96% oxygen, and 0.92% argon by volume according to the U.S. National Institute of Standards and Technology (NIST) standard air model.[15] The molecular weight of dry air is 28.95849 kg/kmol based on the carbon-12 scale. The molecular weight of water is 18.01528 kg/kmol. The ratio of the molecular weight of dry air to the molecular weight of water is 0.622107.

Moist air is treated as mixture of two real gases designated by a subscripts, a and w for dry air and water vapor, respectively. The P–v–T equation for each component and mixture is described by a virial equation of state

$$Z = P\bar{v}/\bar{R}T = 1 + B_{ii}/\bar{v} + C_{iii}/\bar{v}^2 + \cdots \quad (1)$$

Higher-order virial coefficients are assumed to be negligible. The virial coefficients are functions of temperature, and they account for the deviation of actual gases from ideal gases. In the limit when neighboring gas molecules do not interact in any way, all virial coefficients vanish, and Eq. (1) reduces to the ideal-gas law.

The subscript m is used to replace the i to indicate the mixture of dry air and water vapor. For an air–water vapor mixture, one has

$$B_m = x_a^2 B_{aa} + 2x_a x_w B_{aw} + x_w^2 B_{ww} \quad (2)$$

$$C_m = x_a^3 C_{aaa} + 3x_a^2 x_w C_{aaw} + 3x_a x_w^2 C_{aww} + x_w^3 C_{www} \quad (3)$$

Once B_m and C_m are determined, the molar volume, molar enthalpy, and molar entropy of moist air can be evaluated.

The compressibility factor for moist air is defined by Eq. (1), where $Z = 1$ corresponds to an ideal gas. The molar specific volume is obtained by a numerical solution of Eq. (1) for known values of P, T, x_a, and x_w.

Virial Coefficients

Virial coefficient data were fit to polynomial equations as a function of temperature from −100 to 400°C (173 to 673 K) (Ref. 12). The percent error between the equations and the data was less than 0.30% at each data point for each virial coefficient, except for C_{www}, where the error was as high as 2% at a few points. The most up-to-date data for B_{aa} and C_{aaa} are from Lemmon et al.[15] Values for B_{ww} and C_{www} were extracted from Harvey et al.[16] No data could be found in the literature for the cross virial coefficients B_{aw}, C_{aaw}, and C_{aww} at high temperatures, so that the cross virial coefficients were assumed to be given by extending the equations used by Hyland and Wexler[8,9] up to 400°C. Values of the virial coefficients and their temperature derivatives are tabulated as a function of temperature in Ref. 12.

Limited experimental data for B_{aw}, C_{aaw}, and C_{aww} are available at temperatures up to 75°C from Wylie and Fischer.[17] The Wylie and Fischer data are slightly different than the curve-fit data, but they have the same trends as shown in Figs. 1 and 2. The curve fit for B_{aw} agrees well with the experimental data. The experimental data for C_{aaw} have a large uncertainty, and the curve fit is outside the experimental error bounds. Table 1 shows examples of the percentage change in Z due to changing B_{aw}, C_{aaw}, and C_{aww}. It gives the correct value of Z and the percentage change in Z ($= 100(Z - Z')/Z$, where Z' is the value of Z for the changed value of the virial coefficient), for two cases: 1) one cross virial coefficient and its temperature derivative set to 0, others unchanged, and 2) one cross virial

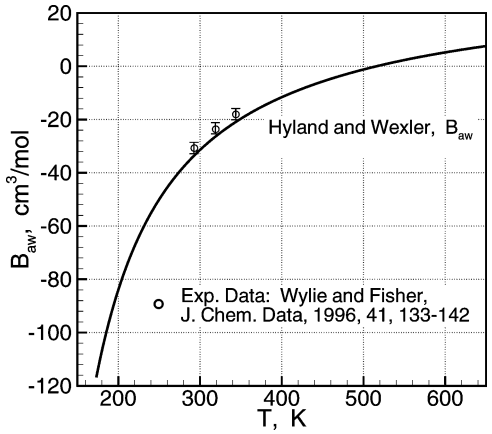

Fig. 1 Cross virial coefficient B_{aw}.

Table 1 Sensitivity of Z to cross virial coefficients

		% change in Z					
t,°C	Z	$B_{aw}=0$	$C_{aaw}=0$	$C_{aww}=0$	$100B_{aw}$	$100C_{aaw}$	$100C_{aww}$
			$W=0.01\ kg_w/kg_{da}$, $P=2.0$ MPa				
70.3	0.99986	−0.042	0.002	−0.002	4.39	−0.163	0.174
200	1.00614	−0.005	0.001	0.000	0.474	−0.072	0.016
400	1.00730	0.010	0.000	0.000	−0.923	−0.032	0.002
			$W=0.10\ kg_w/kg_{da}$, $P=2.0$ MPa				
130.8	0.99744	−0.147	0.007	−0.034	17.7	−0.721	3.60
200	1.00233	−0.037	0.005	−0.011	3.80	−0.486	1.08
400	1.00577	0.073	0.002	−0.011	−6.72	−0.218	0.113
			$W=1.0\ kg_w/kg_{da}$, $P=2.0$ MPa				
189.2	0.95059	−0.117	0.005	−0.138	13.5	−0.563	19.3
200	0.95629	−0.085	0.005	−0.115	9.32	−0.520	16.4
400	0.99260	0.150	0.002	−0.011	−13.1	−0.203	1.07
			$W=0.10\ kg_w/kg_{da}$, $P=0.101325$ MPa				
52.6	0.99912	−0.020	0.000	0.000	2.07	−0.003	0.046
200	1.00011	−0.002	0.000	0.000	0.187	−0.001	0.003
400	1.00029	0.004	0.000	0.000	−0.368	−0.001	0.000
			$W=1.0\ kg_w/kg_{da}$, $P=0.101325$ MPa				
87	0.99282	−0.027	0.000	−0.002	2.76	−0.002	0.187
200	0.99803	−0.004	0.000	0.000	0.374	−0.001	0.025
400	0.99963	0.007	0.000	0.000	−0.728	−0.001	0.003

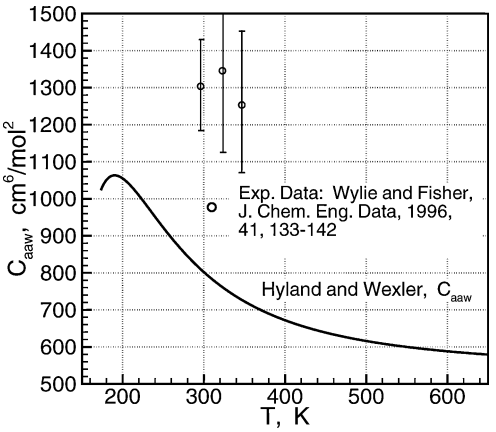

Fig. 2 Cross virial coefficient C_{aaw}.

coefficient and its temperature derivative multiplied by a factor of 100, others unchanged. Results are given at $P=2$ MPa for $W=1$, 0.1, and 0.01 and at $P=1$ atm for $W=1$ and 0.1. The change in the enhancement factor due to changing B_{aw}, C_{aaw}, and C_{aww} was not accounted for in these calculations. When the cross virials are increased by a factor of 100, the percentage change in Z becomes large, especially at large values of W. The virial coefficient sensitivity of $\bar{v}$ is the same as that of Z, and the sensitivity of enthalpy and entropy to changes in the virial coefficients is less than that of Z. The largest uncertainties in our psychrometric calculations are due to the cross virials that are being extrapolated far beyond the range of the limited data available, but Table 1 shows that the cross virial uncertainty on Z is small, except at high values of W and P and only when the cross virials are increased by a factor of 100 from their extrapolated values. The uncertainties due to the cross virials may be more important for other properties close to saturation, which depend on the enhancement factor, such as enthalpy, entropy, and dew point, and the uncertainties will become larger at higher pressures.

Water Properties

The International Association for the Properties of Water and Steam (IAPWS) has the most up-to-date data for the thermodynamic properties of water and steam. In 1997, IAPWS adopted a new formulation for the formulation for the thermodynamic properties of water and steam.[18,19] The IAPWS formulation is developed in terms of the Gibbs function, and properties are generated by taking derivatives of the Gibbs function. Properties of interest are specific volume $v=(\partial g/\partial P)_T$, enthalpy $h=g-T(\partial g/\partial T)_P$, and entropy $s=-(\partial g/\partial T)_P$. The new IAPWS formulation significantly improved both the accuracy and speed of calculation for thermodynamic properties of water and steam. The IAPWS formulation for the properties of water and steam are used in this research.

Superheated Water Vapor

In the superheated region, the Gibbs function is separated into two parts, an ideal-gas part and a residual part. In the current research, the residual part is evaluated using the virial coefficients. The IAPWS equation for the ideal-gas part of the nondimensional Gibbs function is

$$\gamma^\circ = \frac{\bar{g}_{ig}(P,T)}{\bar{R}T} = \ln\pi + \sum_{i=1}^{9} n_i^\circ \tau^{J_i^\circ} \tag{4}$$

where $\pi=P/P^*$ and $\tau=T^*/T$, where $T^*=540$ K and $P^*=1$ MPa. The coefficients n_i° and J_i°, for $i=1,9$, are given in Refs. 18 and 19.

The equations for the ideal-gas properties in molar units are

$$\bar{v}_{ig,w} = \bar{R}T/P \tag{5}$$

enthalpy

$$\bar{h}^\circ_{ig,w} = \bar{R}T\tau \sum_{i=1}^{9} n_i^\circ J_i^\circ \tau^{J_i^\circ - 1} \tag{6}$$

and entropy

$$\bar{s}^\circ_{ig,w} = \bar{R}\left[\tau \sum_{i=1}^{9} n_i^\circ J_i^\circ \tau^{J_i^\circ - 1} - \gamma^\circ\right] \tag{7}$$

Liquid Water

The equation for the Gibbs function in the liquid region is written as

$$\frac{\bar{g}_L(P,T)}{\bar{R}T} = \sum_{i=1}^{34} n_i (7.1-\pi^*)^{I_i} (\tau^* - 1.222)^{J_i} \tag{8}$$

where, $\pi^*=P/P^{**}$ and $\tau^*=T^{**}/T$, where $T^{**}=1386$ K and $P^{**}=16.53$ MPa. The coefficients, n_i, I_i, and J_i are given in Refs. 18 and 19. Liquid thermodynamic properties for $T\geq 273$K (v_L, h_L, and s_L) can be obtained from Eq. (8).

Water Vapor Saturation Pressure

Water vapor saturation pressure is required to determine the dew point and the humidity ratio of moist air. Data for the water vapor saturation pressure over ice (sublimation process) for the temperature range $213.15 \le T \le 273.15$ K ($-60 \le t \le 0°$C) are taken from Sonntag et al.[20] and Olivieri et al.[10] Saturation pressure as a function of temperature for the temperature range $213.15 \le T \le 273.15$ K ($-60 \le t \le 0°$C)is given by

$$P_s = \exp[29.093178 - 2.860529 \times 10^{-9} T^3 - 6178.67/T] \quad (9)$$

in units of pascal. The equation for water vapor saturation pressure for the temperature range $273.15 \le T \le 647.10$ K ($0 \le t \le 374°$C) is taken from IAPWS as

$$P_s = P_1 \left[2C \Big/ \left(-B + \sqrt{B^2 - 4AC}\right)\right]^4 \quad (10)$$

where A, B, and C are defined in terms of Q as

$$Q = T/T_1 - 0.238555576/(T/T_1 - 650.175348)$$

$$A = Q^2 + 1167.05215Q - 724{,}213.167$$

$$B = -17.0738469Q^2 + 12{,}020.8247Q - 3{,}232{,}555.03$$

$$C = 14.9151086Q^2 - 4823.26574Q + 405{,}113.405$$

and where $P_1 = 1.0 \times 10^6$ Pa and $T_1 = 1$ K.

Air Properties

Thermodynamic properties of air are taken from the NIST formulation presented in Refs. 15 and 21. The NIST data are valid for temperatures up to 2000 K and pressures up to 70 MPa. The ideal-gas data for $\bar{h}_{ig,a}$ and $\bar{s}_{ig,a}$ were obtained from the NIST data at small pressures, where $Z = 1$ (to four decimal places) and where the enthalpy data did not change with pressure for temperatures between -100 and 400°C. This occurred near $P = 10$ Pa. The value of $\bar{C}_P$ at $P = 10$ Pa was curve fit vs temperature and integrated to obtain $\bar{h}^\circ_{ig,a}$ and $\bar{s}^\circ_{ig,a}$. The resulting equations are

$$\begin{aligned}\bar{h}^\circ_{ig,a} = {} & 28.921316(T - T_\circ) + 2.5861872 \times 10^{-3}\left(T^2 - T_\circ^2\right)/2 \\ & - 1.9010204 \times 10^{-5}\left(T^3 - T_\circ^3\right)/3 + 5.1208717 \\ & \times 10^{-8}\left(T^4 - T_\circ^4\right)/4 - 3.2775941 \\ & \times 10^{-11}\left(T^5 - T_\circ^5\right)/5 + 8.0457 \end{aligned} \quad (11)$$

$$\begin{aligned}\bar{s}^\circ_{ig,a} = {} & 28.921316\,\ell n(T/T_\circ) + 2.5861872 \times 10^{-3}(T - T_\circ) \\ & - 1.9010204 \times 10^{-5}\left(T^2 - T_\circ^2\right)/2 + 5.1208717 \\ & \times 10^{-8}\left(T^3 - T_\circ^3\right)/3 - 3.2775941 \\ & \times 10^{-11}\left(T^4 - T_\circ^4\right)/4 + 0.02393 \end{aligned} \quad (12)$$

In these equations, $T_\circ = 273.15$ K. Equation (12) for $\bar{s}^\circ_{ig,a}$ is valid at $P = 101{,}352$ Pa. In other words, the constant (0.02393) in Eq. (12) contains the pressure adjustment from $P = 10$ Pa to 1 atm. In addition, the constants in Eqs. (11) and (12) make $\bar{h}_a$ and $\bar{s}_a$ zero at $P = 101{,}325$ Pa and $t = 0°$C, when the virial coefficient real-gas corrections are accounted for.

Thermodynamic Properties

Moist air thermodynamic properties are formulated as a function of an ideal-gas value plus the real-gas correction.

Enthalpy

The molar enthalpy (kJ/kmol) for dry air, $i = a$, or water vapor, $i = w$, is

$$\bar{h}_i = \bar{h}^\circ_{ig,i} + \bar{R}T\left[\left(B_{ii} - T\frac{dB_{ii}}{dT}\right)\frac{1}{\bar{v}_i} + \left(C_{iii} - \frac{1}{2}T\frac{dC_{iii}}{dT}\right)\frac{1}{\bar{v}_i^2}\right] \quad (13)$$

In the virial equation of state formulation, the real-gas correction is added to the value of $\bar{h}^\circ_{ig,i}$. The reference state for water vapor is $\bar{h}_w = 0$ for saturated liquid water at $t = 0°$C, and the reference state for air is $\bar{h}_a = 0$ at $t = 0°$C and $P = 101{,}325$ Pa.

The molar enthalpy (kJ/kmol) of moist air is

$$\begin{aligned}\bar{h}_m = {} & x_a\bar{h}^\circ_{ig,a} + x_w\bar{h}^\circ_{ig,w} + \bar{R}T\left[\left(B_m - T\frac{dB_m}{dT}\right)\frac{1}{\bar{v}_m}\right. \\ & \left. + \left(C_m - \frac{1}{2}T\frac{dC_m}{dT}\right)\frac{1}{\bar{v}_m^2}\right] \end{aligned} \quad (14)$$

The derivatives of B_m and C_m are obtained directly from their curve-fit equations. The ideal-gas terms $\bar{h}_{ig,w}$ and $\bar{h}_{ig,a}$ are evaluated from Eqs. (6) and (11), respectively. The IAPWS data are a function of both temperature and pressure, so that the water vapor partial pressure in moist air is assumed to be $P_w = x_w P$.

Entropy

The equation for dry air entropy is

$$\begin{aligned}\bar{s}_a = {} & \bar{s}^\circ_{ig,a} + \bar{R}\left\{-\ell n\frac{P}{P^\circ} + \ell n\left(\frac{P\bar{v}_a}{\bar{R}T}\right) - \left[\left(B_{aa} + T\frac{dB_{aa}}{dT}\right)\frac{1}{\bar{v}_a}\right.\right. \\ & \left.\left. + \left(C_{aaa} + T\frac{dC_{aaa}}{dT}\right)\frac{1}{2\bar{v}_a^2}\right]\right\} \end{aligned} \quad (15)$$

where $\bar{s}^\circ_{ig,a}$ is given by Eq. (12). Recall that the constant in Eq. (12) contains the pressure correction to 1 atm and makes $\bar{s}_a = 0$ at $t = 0°$C. In other words, at $P = 101{,}325$ Pa and $t = 0°$C, Eq. (12) gives $\bar{s}^\circ_{ig,a} = 0.02393$ kJ/(kmol · K) and Eq. (15) gives $\bar{s}_a = 0$.

The equation for water vapor entropy in the virial coefficient formulation is

$$\begin{aligned}\bar{s}_w = {} & \bar{s}^\circ_{ig,w} + \bar{R}\left\{-\ell n\frac{P_w}{P^\circ} + \ell n\frac{P_w\bar{v}_w}{\bar{R}T} - \left[\left(B_{ww} + T\frac{dB_{ww}}{dT}\right)\frac{1}{\bar{v}_w}\right.\right. \\ & \left.\left. + \left(C_{www} + T\frac{dC_{www}}{dT}\right)\frac{1}{2\bar{v}_w^2}\right]\right\} \end{aligned} \quad (16)$$

where $\bar{s}^\circ_{ig,w}$ is the value of entropy from the ideal-gas IAPWS data as given by Eq. (7).

The molar entropy of moist air, $\bar{s}_m$, is

$$\begin{aligned}\bar{s}_m = {} & x_a\bar{s}^\circ_{ig,a} + x_w\bar{s}^\circ_{ig,w} + \bar{R}\left\{-\ell n\frac{P}{P^\circ} + x_a\,\ell n\frac{P\bar{v}_m}{x_a\bar{R}T} + x_w\,\ell n\frac{P\bar{v}_m}{x_w\bar{R}T}\right. \\ & \left. - \left[\left(B_m + T\frac{dB_m}{dT}\right)\frac{1}{\bar{v}_m} + \left(C_m + T\frac{dC_m}{dT}\right)\frac{1}{2\bar{v}_m^2}\right]\right\} \end{aligned} \quad (17)$$

Saturated Moist Air

Moist air is saturated when it is in contact and in neutral equilibrium with a flat surface of pure condensed liquid water. The saturation data for moist air is a function of temperature, pressure, and saturation humidity ratio. In the saturated state, the mole fractions of water vapor, x_{ws}, and of air, x_{as}, are

$$x_{ws} = fP_s/P \quad (18)$$

$$x_{as} = (P - fP_s)/P \quad (19)$$

The enhancement factor f is a function of P and T, and it accounts for the nonideal behavior of the water vapor–air mixture in the saturated state. Here f accounts for the effect of pressure and dissolved gases on the properties of the condensed phase and the effect of intermolecular forces on properties of the moisture itself. Factor f is related to the thermodynamic parameters of the state, the virial coefficients, and several physical constants as given in Refs. 8–10 and 12. Representative values of f are given in Table 2 as a function of T at a constant value of either P or altitude. Note that $f = 1$ for all superheated states.[12]

The saturation humidity ratio for moist air at a temperature T and pressure P is

$$W_s = (M_w/M_a)[f P_s/(P - f P_s)] \tag{20}$$

where P_s is the saturation vapor pressure at temperature T.

Humidity Ratio and Relative Humidity

The humidity ratio is

$$W = M_w/M_a(x_w/x_a) = 0.6221070(x_w/x_a) \tag{21}$$

The percent relative humidity ϕ is defined as

$$\phi = 100x_w P/(f P_s) \tag{22}$$

for $P \le f P_s$, otherwise ϕ is undefined.

Wet-Bulb Temperature

The thermodynamic wet-bulb temperature, denoted by t_{wb}, is defined as the solution to the energy balance equation at a specific value of pressure

$$h_s(t_{wb}) = h(t, W) + [W_s(t_{wb}) - W]h_{l,w}(t_{wb}) \tag{23}$$

Table 2 Values of f

t,°C	101.325 kPa	200 kPa	500 kPa	1 MPa	2 MPa	3 km	10 km	20 km
−60	1.00635	1.01265	1.03213	1.06587	1.13834	1.00378	1.00175	0.99994
−40	1.00519	1.01023	1.02578	1.05249	1.10886	1.00359	1.00138	1.00031
−20	1.00444	1.00856	1.02127	1.04293	1.08822	1.00307	1.00125	1.00037
0	1.00400	1.00744	1.01802	1.03594	1.07321	1.00292	1.00139	1.00063
20	1.00403	1.00694	1.01585	1.03092	1.06211	1.00319	1.00184	1.00081
40	1.00476	1.00729	1.01489	1.02776	1.05424	1.00393	1.00238	1.00000
60	1.00589	1.00852	1.01532	1.02656	1.04947	1.00469	1.00138	1.00000
80	1.00575	1.00981	1.01698	1.02730	1.04774	1.00327	1.00000	1.00000
100	1.00000	1.00878	1.01888	1.02950	1.04873	1.00000	1.00000	1.00000
120	1.00000	1.00038	1.01850	1.03174	1.05152	1.00000	1.00000	1.00000
140	1.00000	1.00000	1.01103	1.03117	1.05422	1.00000	1.00000	1.00000
160	1.00000	1.00000	1.00000	1.02303	1.05378	1.00000	1.00000	1.00000
180	1.00000	1.00000	1.00000	1.00000	1.04572	1.00000	1.00000	1.00000
200	1.00000	1.00000	1.00000	1.00000	1.02399	1.00000	1.00000	1.00000

Table 3 Psychrometric properties near the saturated state

t, °C	t_{wb}, °C	t_{dp}, °C	ϕ, %	P_v, Pa	W, kg_w/kg_{da}	h, kJ/kg_{da}	v, m^3/kg_{da}	s, $kJ/K \cdot kg_{da}$
				P = 101,325 Pa, sea level				
25	25	25.00	100.0	3169.75	0.02018	76.517	0.8719	0.26983
25	20	17.60	63.5	2013.21	0.01266	57.401	0.8617	0.20488
25	15	7.73	33.2	1053.72	0.00656	41.873	0.8535	0.15062
25	10	−10.39	7.9	251.37	0.00155	29.111	0.8467	0.10392
				P = 200,000 Pa				
25	25	25.00	100.0	3169.75	0.01009	50.604	0.4346	−0.01692
25	20	14.86	53.3	1690.43	0.00534	38.521	0.4314	−0.05813
25	15	−4.73	13.0	411.39	0.00129	28.215	0.4286	−0.09495
				P = 500,000 Pa				
25	25	25.00	100.0	3169.75	0.00403	34.491	0.1720	−0.33663
25	20	2.15	22.5	713.82	0.00090	26.540	0.1712	−0.36415
				P = 70,108 Pa, altitude = 3 km				
25	25	25.00	100.0	3169.75	0.02956	100.490	1.2786	0.46025
25	20	18.39	66.7	2115.53	0.01942	74.685	1.2588	0.37267
25	15	10.35	39.7	1257.27	0.01140	54.256	1.2431	0.30166
25	10	−1.16	17.5	555.12	0.00498	37.915	1.2305	0.24298
				P = 26,500 Pa, altitude = 10 km				
25	25	25.00	100.0	3169.75	0.08471	241.037	3.6690	1.23510
25	20	19.44	71.3	2258.64	0.05809	173.266	3.5312	1.00545
25	15	13.44	48.6	1541.92	0.03852	123.427	3.4298	0.83333
25	10	6.67	30.9	979.82	0.02393	86.294	3.3542	0.70232
25	5	−1.50	17.0	539.31	0.01295	58.316	3.2972	0.60101
25	0	−10.80	7.6	242.44	0.00576	39.989	3.2599	0.53241
				P = 5529.3 Pa, altitude = 20 km				
25	25	25.00	100.0	3169.75	0.83711	2157.103	36.2795	8.33123
25	20	19.93	73.5	2328.42	0.45310	1179.361	26.7433	5.02271
25	15	14.76	53.0	1679.96	0.27178	717.648	22.2388	3.43344
25	10	9.47	37.4	1185.10	0.16986	458.083	19.7058	2.52404
25	5	3.96	25.6	811.06	0.10703	298.034	18.1436	1.95275
25	0	−1.48	17.0	540.38	0.06744	197.180	17.1591	1.58560
25	−5	−7.88	9.9	313.72	0.03745	120.781	16.4131	1.30106

where $h(t, W)$ is the enthalpy of moist air at dry-bulb temperature t and humidity ratio W, $h_s(t_{wb})$ is the enthalpy of moist saturated air at the wet-bulb temperature t_{wb}, $W_s(t_{wb})$ is the saturation humidity ratio of water at temperature t_{wb}, and $h_{l,w}(t_{wb})$ is the enthalpy of liquid water at temperature t_{wb}. Equation (23) is solved numerically to obtain t_{wb} as a function of t and W.

Psychrometric Charts

Psychrometric charts were constructed at a specific pressure using computer software.[12] The charts were generated using data along lines of constant h in an x–y orthogonal coordinate system. At each moist air state (h, W), which corresponds to an x–y point on the chart grid, all of the necessary data (t, t_{wb}, v, ϕ, and Z) were generated numerically. The h axis was set at an angle with respect to the x axis. Lines of constant h are straight lines. The W axis was parallel to the y axis and located on the right-hand side of the graph. The maximum dry-bulb temperature, $t = 400°C$, was taken to be along the right-hand ordinate, or W axis, so that the $t = 400°C$ temperature line was vertical. Previous psychrometric charts using h and W as nonorthogonal axes were constructed with either the maximum t or a dry-bulb temperature close to the maximum value as a vertical line.[8–10] Lower values of t fan out to the left. Contour plots in the x–y coordinate system were made for each variable (h, t, t_{wb}, v, ϕ, and Z), by putting a single variable on a single frame. The frames are stacked on top of each other and are transparent so that the contours plots show through. The seven frames from top to bottom contain h, t, t_{wb}, v, ϕ, Z, and the chart grid, respectively.

Results and Discussion

Previous to this research project, psychrometric charts were only available for dry-bulb temperatures up to 200°C and humidity ratios between 0 and 0.09 kg_w/kg_a at sea-level pressure and for

Table 4 Thermodynamic properties of saturated moist air: Altitude

	Humity ratio, W_s	Volume, m^3/kg_{da}		Enthalpy, kJ/kg_{da}		Entropy, $kJ/kg_{da} \cdot K$		
t, °C	kg_w/kg_{da}	v_{da}	v_s	h_{da}	h_s	s_{da}	s_s	Z
			$P = 101.325$ kPa (sea level), $t_s = 100°C$					
0	0.00379	0.7735	0.7782	0.00	9.476	0.0000	0.0364	0.9994
20	0.01476	0.8304	0.8500	20.122	57.568	0.0711	0.2057	0.9996
40	0.04915	0.8872	0.9570	40.257	166.720	0.1375	0.5650	0.9998
60	0.15360	0.9439	1.1755	60.411	461.034	0.1999	1.4773	0.9999
80	0.55310	1.0007	1.8814	80.591	1542.234	0.2587	4.6491	1.0000
			$P = 70.108$ kPa (3 km), $t_s = 90°C$					
0	0.00549	1.118	1.128	0.09	13.81	0.1060	0.1587	0.9996
20	0.02154	1.200	1.242	20.20	74.85	0.1770	0.3735	0.9997
40	0.07356	1.282	1.433	40.32	229.60	0.2434	0.8826	0.9999
60	0.24899	1.364	1.907	60.47	709.96	0.3058	2.3708	0.9999
			$P = 26.50$ kPa (10 km), $t_s = 66.3°C$					
0	0.01471	2.959	3.029	0.21	37.0	0.3857	0.5270	0.9998
20	0.06035	3.176	3.483	20.30	173.4	0.4567	1.0062	0.9999
40	0.24112	3.393	4.704	40.41	660.9	0.5230	2.6073	0.9999
			$P = 5.5293$ kPa, (20 km), $t_s = 34.7°C$					
0	0.07737	14.183	15.946	0.26	193.8	0.8358	1.5778	1.0000
10	0.17782	14.702	18.901	10.30	458.3	0.8719	2.5266	1.0000
20	0.45682	15.222	26.384	20.35	1179.5	0.9068	5.0235	1.0000
			$P = 0.20$ MPa, $t_s = 120.2°C$					
0	0.00192	0.392	0.393	−0.27	4.53	−0.1961	−0.1776	0.9988
20	0.00741	0.421	0.426	19.89	38.69	−0.1249	−0.0573	0.9993
40	0.02403	0.449	0.467	40.05	101.86	−0.0583	0.1508	0.9996
60	0.06957	0.478	0.531	60.23	241.64	0.0042	0.5843	0.9999
80	0.19581	0.507	0.665	80.44	597.76	0.0630	1.6306	1.0001
100	0.65150	0.536	1.087	100.67	1843.38	0.1188	5.1123	1.0002
			$P = 0.50$ MPa, $t_s = 151.8°C$					
0	0.0008	0.156	0.157	−1.09	0.85	−0.4616	−0.4542	0.9971
20	0.0030	0.168	0.169	19.18	26.70	−0.3900	−0.3630	0.9982
40	0.0095	0.180	0.182	39.44	63.76	−0.3232	−0.2408	0.9990
60	0.0263	0.191	0.199	59.70	128.12	−0.2605	−0.0413	0.9997
80	0.0664	0.203	0.224	79.97	255.26	−0.2014	0.3322	1.0002
100	0.1621	0.214	0.269	100.26	533.44	−0.1455	1.1106	1.0006
120	0.4229	0.226	0.375	120.58	1264.06	−0.0924	3.0662	1.0009
			$P = 1.0$ MPa, $t_s = 179.9°C$					
0	0.0004	0.078	0.078	−2.45	−1.46	−0.6648	−0.6610	0.9944
20	0.0015	0.084	0.084	18.01	21.81	−0.5925	−0.5789	0.9966
40	0.0048	0.090	0.090	38.42	50.62	−0.5252	−0.4839	0.9982
60	0.0130	0.096	0.098	58.81	92.64	−0.4621	−0.3536	0.9995
80	0.0319	0.101	0.107	79.20	163.18	−0.4026	−0.1467	1.0004
100	0.0725	0.107	0.119	99.59	293.21	−0.3465	0.2168	1.0012
120	0.1604	0.113	0.141	120.00	553.16	−0.2932	0.9123	1.0018
			$P = 2.0$ MPa, $t_s = 212.4°C$					
0	0.0002	0.039	0.039	−5.12	−4.62	−0.8720	−0.8701	0.9894
20	0.0008	0.042	0.042	15.70	17.65	−0.7985	−0.7915	0.9937
40	0.0024	0.045	0.045	36.42	42.64	−0.7301	−0.7090	0.9969
60	0.0066	0.048	0.048	57.08	74.15	−0.6662	−0.6114	0.9994
80	0.0159	0.051	0.052	77.69	119.36	−0.6061	−0.4790	1.0013
100	0.0349	0.054	0.057	98.28	191.33	−0.5494	−0.2783	1.0027
120	0.0726	0.057	0.063	118.86	314.35	−0.4956	0.0501	1.0039
140	0.1465	0.060	0.073	139.46	538.20	−0.4445	0.6246	1.0048
160	0.3005	0.063	0.091	160.07	985.87	−0.3958	1.7333	1.0055

$0 \le t \le 50°C$, $0 \le W \le 0.03$ at pressures corresponding to altitudes of 750, 1500, and 2250 m. The current calculations agree with the previous data at $t = 200°C$ for $0 \le W \le 0.09$ to within $\pm 0.5\%$ (Refs. 12 and 13). The data presented herein extend the dry-bulb temperatures to 400°C and the humidity ratio up to 1 kg_w/kg_a and covers a range of pressures from 2 MPa to 5529.3 Pa (altitude of 20 km). Additional data are available in Ref. 12.

Table 3 gives psychrometric properties t_{dp}, ϕ, vapor pressure, W, h, v, and s as a function of t_{wb} at $t_{db} = 25°C$ for moist air near the saturated state, $\phi = 100\%$. Table 3 contains data for several different pressures, or altitudes. The sea-level data shown in Table 3 agree to within $\pm 0.5\%$ with the previous data (Table 20 of Olivieri et al.[10]). The data in Table 3 at pressures of 0.2 and 0.5 MPa and altitudes of 3, 10, and 20 km are new. The state point data have been calculated using the formulation developed in this paper. The data can be used to judge the accuracy of future calculations.

Table 4 presents the saturation values W_s, v_{da}, v_s, h_{da}, h_s, s_{da}, s_s, and Z as a function of saturation temperature at altitudes of sea level, 3, 10, and 20 km and at pressures of 0.2, 0.5, 1, and 2 MPa.

Table 5 presents state point properties t_{wb}, v, h, s, and Z at sea-level pressure as a function of W for $t = 200$ and 400°C. These data are given to allow comparison to future work.

The new and extended data are presented in psychrometric charts. Figure 3 shows the psychrometric chart at sea level for $0 \le t \le 400°C$ and $0 \le W \le 1$ kg_w/kg_{da}. It shows data for t, t_{wb}, v, ϕ, Z, and h as a function of W. The extended dry-bulb temperature and humidity ratio ranges distort the chart to the left relative to lower temperature charts. The distortation can be reduced slightly by increasing the slope of the constant h lines during the chart construction.

Figure 4 shows the psychrometric chart for a pressure of 2 MPa for $0 \le t \le 400°C$ and $0 \le W \le 1$ kg_w/kg_{da}. The saturation temperature at 2 MPa is 212.4°C.

Figure 5 shows the psychrometric chart for an altitude of 20 km for $0 \le t \le 400°C$ and $0 \le W \le 1$ kg_w/kg_{da}. The saturation temperature at 2 km is approximately 33°C.

The psychrometric charts graphically show the moist air data over a very large property range, which makes them somewhat hard to read. The left boundary is the saturation line, and $t_{db} = 400°C$ is the right boundary. Lines of constant enthalpy are labeled on the left and angle downward to the right. Lines of constant dry-bulb temperature are labeled on the y axis and angle to the left for increasing values of W. The lines for constant t_{wb} are dashed lines and are almost parallel to the constant h lines. Lines for constant v are solid lines that slope downward to the right. The constant relative humidity

Table 5 State data at $P = 101.325$ kPa

W, kg_w/kg_{da}	t_{wb}, °C	v, m^3/kg_{da}	h, kJ/kg_{da}	s, $kJ/K \cdot kg_{da}$	Z
		$t_{db} = 200°C$, $t_s = 100°C$			
0.00	45.07	1.341	202.57	0.5560	1.0003
0.10	61.85	1.556	490.47	1.4735	1.0001
0.20	69.95	1.771	778.29	2.3334	0.9998
0.30	74.99	1.986	1066.04	3.1746	0.9996
0.40	78.50	2.201	1353.75	4.0051	0.9993
0.50	81.11	2.416	1641.43	4.8284	0.9990
0.60	83.14	2.631	1929.09	5.6465	0.9988
0.70	84.76	2.845	2216.73	6.4606	0.9986
0.80	86.09	3.060	2504.35	7.2715	0.9984
0.90	87.20	3.274	2791.96	8.0799	0.9982
1.00	88.15	3.489	3079.56	8.8862	0.9980
		$t_{db} = 400°C$, $t_s = 100°C$			
0.00	59.50	1.908	411.76	0.9243	1.0004
0.10	69.72	2.215	739.72	1.9123	1.0003
0.20	75.52	2.521	1067.66	2.8428	1.0002
0.30	79.35	2.828	1395.57	3.7547	1.0001
0.40	82.10	3.134	1723.48	4.6559	1.0000
0.50	84.19	3.440	2051.37	5.5500	0.9999
0.60	85.83	3.747	2379.26	6.4389	0.9999
0.70	87.15	4.053	2707.14	7.3238	0.9998
0.80	88.25	4.359	3035.02	8.2056	0.9997
0.90	89.17	4.665	3362.89	9.0849	0.9997
1.00	89.95	4.972	3690.76	9.9621	0.9996

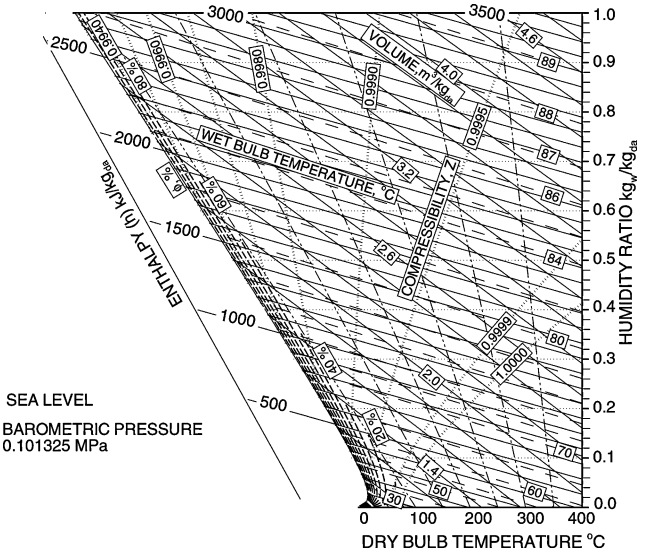

Fig. 3 Psychrometric chart for sea level, $P = 101.325$ kPa.

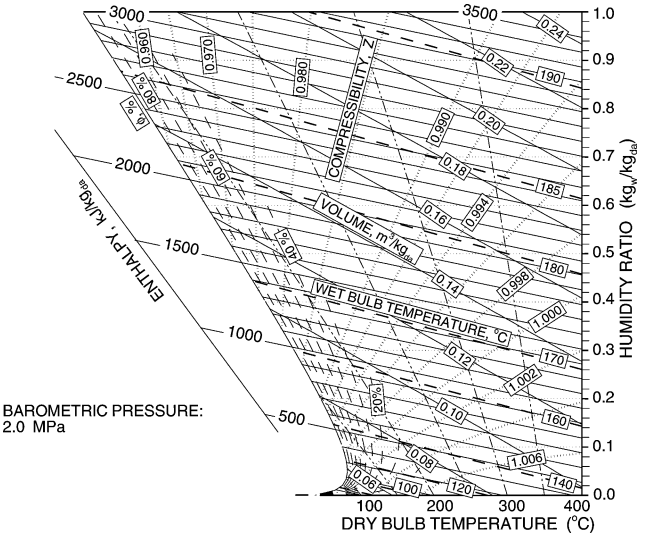

Fig. 4 Psychrometric chart, $P = 2$ MPa.

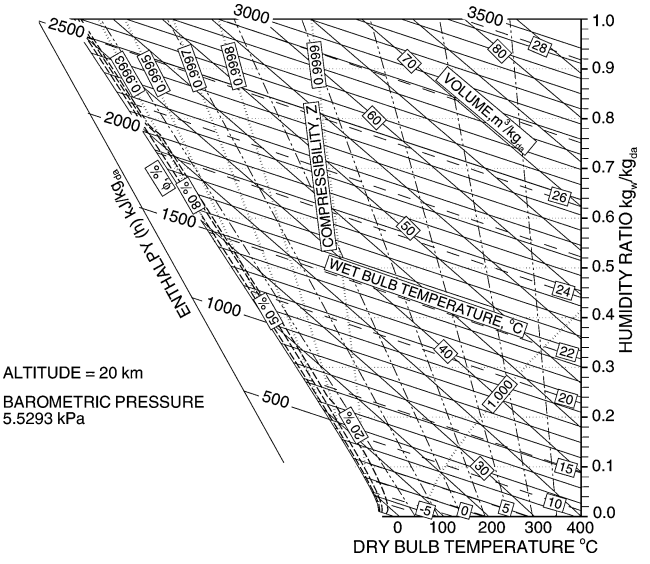

Fig. 5 Psychrometric chart for altitude = 20 km and $P = 5.5293$ kPa.

lines are dashed and are located on the left side of the chart near the saturation state. The lines of constant Z are dotted lines that fan out from the lower left corner of the chart.

Summary

Equations to predict psychrometric data for moist air are formulated. Psychrometric data for moist air are generated and presented in the form of psychrometric charts for $t_s \leq t \leq 400°C$ and $0 \leq W \leq 1$. The moist air is formulated as a real gas. The data extend the maximum value of W from 0.09 to 1 kg_w/kg_a and extend the maximum dry-bulb temperature from 200 to 400°C. In the development of the thermodynamic properties, the most current data are used for the virial coefficients and the water vapor and air properties.

The accuracy of the predicted data are judged to be better than 1% over the complete range of parameters. The largest uncertainty is in the cross virial coefficients.

References

[1]Oates, G. C., *Aerothermodynamics of Gas Turbine and Rocket Propulsion*, edited by J. S. Przemieniecki (Series Editor-in Chief), Revised and Enlarged, AIAA Education Series, AIAA, Washington, DC, 1988, pp. 312, 313.

[2]Stewart, W. E., "Condensation and Icing in Gas Turbine systems: Inlet Air Temperature and Humidity Limits," *ASHRAE Transactions: Symposia*, Vol. 107, Pt. 1, American Society of Heating, Refrigerating and Air-Conditioning Engineers, Atlanta, 2001, pp. 887–891.

[3]Andrepont, J. S., "Combustion Turbine Inlet Air Cooling (CTIAC): Benefits and Technology Options in District Energy Applications," *ASHRAE Transactions: Symposia*, Vol. 107, Pt. 1, American Society of Heating, Refrigerating and Air-Conditioning Engineers, Atlanta, 2001, pp. 892–899.

[4]Tanatsugu, N., Sato, T., Balepin, V., Naruo, Y., Mizutani, T., Kashiwagi, T., Hamabe, K., Tomike, J., and Minami, R., "Development Study on ATREX Engine," *Acta Astronautica*, Vol. 41, No. 12, 1998, pp. 851–862.

[5]Balepin, V. V., and Liston, G. W., "The SteamJet: Mach 6+ Turbine Engine with Inlet Air Conditioning," AIAA Paper 2001-3238, July 2001.

[6]Cramer, O., "The Variation of the Specific Heat Ratio and the Speed on Sound in Air with Temperature, Pressure, Humidity, and CO_2 Concentration," *Journal of the Acoustical Society of America*, Vol. 93, No. 5, 1993, pp. 2510–2516.

[7]Crassous, J., Bocquet, L., Ciliberto, S., and Laroche, C., "Humidity Effect on Static Aging of Dry Friction," *Europhysics Letters*, Vol. 47, No. 5, 1999, pp. 562–567.

[8]Hyland, R. W., and Wexler, A., "Formulation for the Thermodynamic Properties of Dry Air from 173.15 K to 473.15 K, and of Saturated Moist Air from 173.15 K to 372.15 K, at Pressures to 5 MPa," *ASHRAE Transactions,* Vol. 89, Pt. 2A, American Society of Heating, Refrigerating and Air-Conditioning Engineers, Atlanta, 1983, pp. 520–535.

[9]Hyland, R. W., and Wexler, A., "Formulation for the Thermodynamic Properties of the Saturated Phases of H_2O from 173.15 K to 473.15 K," *ASHRAE Transactions*, Vol. 89, Pt. 2A, American Society of Heating, Refrigerating and Air-Conditioning Engineers, Atlanta, 1983, pp. 500–519.

[10]Olivieri, J., Singh, T., and Lovodocky, S., *ASHRAE Psychrometrics—Theory and Practice*, American Society of Heating, Refrigerating and Air-Conditioning Engineers, Inc., Atlanta, 1996, Chap. 1.

[11]Sauer, H. J., Jr., Nelson, H. F., and Huang, X., "The Search for High Temperature Experimental Psychrometric Data," *ASHRAE Transactions*, Vol. 107, Pt. 2, American Society of Heating, Refrigerating and Air-Conditioning Engineers, Atlanta, 2001, pp. 768–779.

[12]Nelson, H. F., and Sauer, H. J., Jr., "Formulation of High Temperature Properties of Moist Air, *International Journal of Heating, Ventilating, Air-Conditioning and Refrigerating Research*, Vol. 8, No. 3, 2002, pp. 311–334.

[13]Nelson, H. F., Sauer, H. J., Jr., and Huang, X., "High Temperature Properties of Moist Air," *ASHRAE Transactions*, Vol. 107, Pt. 2, American Society of Heating, Refrigerating and Air-Conditioning Engineers, Atlanta, 2001, pp. 780–791.

[14]Stewart, R. B., Jacobsen, R. T., and Becker, J. H., 1983. "Formulations for Thermodynamic Properties of Moist Air at Low Pressures as used for Construction of New ASHRAE SI Unit Psychrometric Charts," *ASHRAE Transactions*, Vol. 89, Pt. 2A, American Society of Heating, Refrigerating and Air-Conditioning Engineers, Atlanta, 1983, pp. 536–548.

[15]Lemmon, E. W., Jacobsen, R. T., Penoncello, S. G., and Friend, D. G., "Thermodynamic Properties of Air and Mixtures of Nitrogen, Argon and Oxygen from 60 to 2000 K at Pressures to 2000 MPa," *Journal of Physical and Chemical Reference Data*, Vol. 29, No. 3, 2000, pp. 331–385.

[16]Harvey, A. H., Peskin, A. P., and Klein, S. A., *NIST/ASME Steam Properties Database 10, Users Guide*, National Inst. of Standards and Technology, Boulder, CO, 1997.

[17]Wylie, R. G., and Fischer, R. S., "Molecular Interaction of Water Vapor and Air," *Journal of Chemical Engineering Data*, Vol. 41, No. 1, 1996, pp. 133–142.

[18]Wagner, W., and Kruse, A., *Properties of Water and Steam*, Springer-Verlag, Berlin, 1998.

[19]Wagner, W., Cooper, J. R., Dittmann, A., Kijima, J., Kretzschmar, H.-J., Kruse, A., Mares, R., Oguchi, K., Sato, H., Stocker, I., Sifner, O., Takaishi, Y., Tanishita, I., Trubenbach, J., and Willkommen, T., "The IAPWS Industrial Formulation 1997 for the Thermodynamic Properties of Water and Steam," *Journal of Engineering for Gas Turbines and Power*, Vol. 122, No. 1, 2000, pp. 150–182.

[20]Sonntag, R. E., Borgnakke, C., and VanWylen, G. J., *Foundations of Thermodynamics*, 5th ed., Wiley, New York, 1998, pp. 682, 683.

[21]Jacobsen, R. T., Penoncello, S. G., Beyerlein, S. W., Clarke, W. P., and Lemmon, E. A., "A Thermodynamic Property Formulation for Air," *Fluid Phase Equilibria*, Vol. 79, Nov. 1992, pp. 113–124.